

# Leakage from inclined porous reservoirs

PAWEL J. ZIMOCCH<sup>†</sup>, JEROME A. NEUFELD  
AND DOMINIC VELLA<sup>‡</sup>

Institute of Theoretical Geophysics, Department of Applied Mathematics and Theoretical Physics,  
University of Cambridge, Wilberforce Road, Cambridge CB3 0WA, UK

(Received 15 November 2010; revised 28 January 2011; accepted 8 February 2011;  
first published online 14 March 2011)

We investigate the effect of localized leakage on the storage of buoyant fluids in inclined porous reservoirs, with application to the geological storage of CO<sub>2</sub>. We find that once the current has propagated some distance beyond the point of leakage, its profile becomes steady in time, save for the nose, which advances at a constant speed. Crucially, this steady state implies that the efficiency of storage (defined as the instantaneous proportion of the injected fluid that does not leak) tends to a finite value. This contrasts with previous studies of localized leakage in horizontal reservoirs, which found that the efficiency of storage tends to zero at late times. We analyse the steady-state efficiency and the time scales of evolution for a leakage point located either upslope or downslope of the injection point using analytical and numerical methods. These findings are verified by model laboratory experiments. Finally, we consider the implications of our results for the geological storage of CO<sub>2</sub> under sloping cap rocks compromised by a fracture or fissure.

**Key words:** gravity currents, Hele-Shaw flows

---

## 1. Introduction

Recently, the buoyancy-driven flow of liquids in a porous medium has received renewed interest because of the potential to sequester large amounts of carbon dioxide (CO<sub>2</sub>) in porous reservoirs (Bickle *et al.* 2007). Several small-scale demonstration projects have already commenced, pumping supercritical CO<sub>2</sub> into brine-saturated aquifers to test the viability of this technique. These have confirmed that the CO<sub>2</sub> remains buoyant relative to the ambient brine and so migrates upwards until it encounters a relatively impermeable cap rock after which it spreads horizontally as a ‘gravity current’ (Huppert 2006). The motion of gravity currents without leakage has been extensively studied in both two and three dimensions (see Huppert & Woods 1995; Lyle *et al.* 2005, respectively). The presence of a sloping cap rock causes the current to propagate preferentially along the slope (Vella & Huppert 2006).

For the geological storage of CO<sub>2</sub> to be effective, the relatively impermeable cap rock must prevent the buoyant supercritical fluid from escaping the aquifer for long enough that other, more permanent, mechanisms (e.g. dissolution and capillary trapping) have time to act. It is therefore important to understand the time scale over which the cap rock may retain a substantial proportion of the injected CO<sub>2</sub>. Leakage

<sup>†</sup> Present address: Department of Mechanical Engineering, MIT, Cambridge MA 02139, USA.

<sup>‡</sup> Present address: OCCAM, Mathematical Institute, 24-29 St Giles’, Oxford OX1 3LB, UK.  
Email address for correspondence: dominic.vella@maths.ox.ac.uk

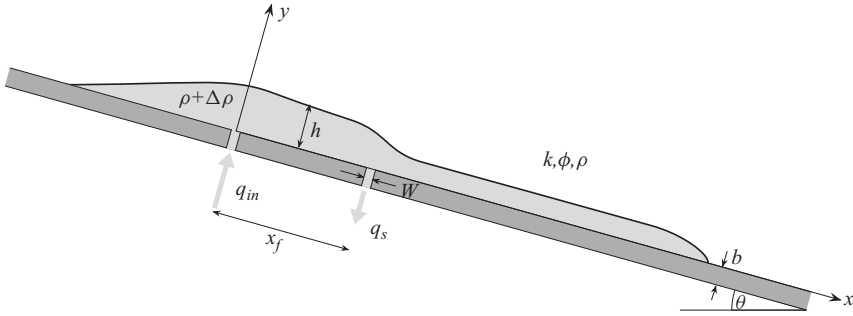


FIGURE 1. Schematic of a gravity current on a slope with a downslope localized leak.

may occur over an extended region because of the small, but finite, permeability of the cap rock (see Pritchard, Woods & Hogg 2001; Woods & Farcas 2009, for example). Alternatively, leakage may be focused in a small region because of the presence of a high-permeability pathway such as a fracture or fissure in the overlying cap rock. Several recent studies have examined localized leakage from horizontal gravity currents in a variety of geometries (Pritchard 2007; Neufeld, Vella & Huppert 2009; Neufeld *et al.* 2011; Vella *et al.* 2011). These studies have been primarily concerned with the rate at which fluid leaks from the reservoir. A convenient way of characterizing this leakage is by using the efficiency of storage,

$$E_s \equiv \frac{q_{in} - q_s}{q_{in}}, \quad (1.1)$$

in which  $q_{in}$  is the volumetric injection flux and  $q_s$  is the volumetric leakage flux. These previous studies have determined the long-time behaviour of  $E_s$  with horizontal boundaries using asymptotic methods. In two dimensions, where fluid is injected along a line and leaks from a line, Neufeld *et al.* (2009) found that  $E_s \propto t^{-1/2}$  at late times. With injection occurring at a point and leakage localized to a small, circular region, Neufeld *et al.* (2011) found that  $E_s \propto 1/\ln t$ , while for injection at a point but leakage along a line Vella *et al.* (2011) found that  $E_s \propto t^{-2/5}$ . In this article, we show that the presence of a sloping cap rock changes these results *qualitatively*: at late times the efficiency of storage tends to a constant,  $E_s \rightarrow E_s^\infty$ . We begin by detailing the theoretical model in §2 before studying the steady state in §3 (including the determination of  $E_s^\infty$ ) and the evolution to this state in §4. We compare these results with analogue laboratory experiments in §5 before concluding in §6 by considering the geological storage of CO<sub>2</sub>.

## 2. Theoretical modelling

### 2.1. Governing equations

Consider a liquid of density  $\rho + \Delta\rho$  and viscosity  $\mu$  injected with constant volume flux per unit width  $q_{in}$  at  $x=0$  into a two-dimensional, semi-infinite porous medium. The porous medium, of constant permeability  $k$  and porosity  $\phi$ , is saturated with a fluid of density  $\rho$  and is bounded below by a layer of thickness  $b$  at an angle  $\theta$  to the horizontal (see figure 1). (We illustrate here the case of a dense fluid propagating at the base of a reservoir for comparison with our experiments. However, the analysis presented is identical to that for a buoyant fluid at the top of a reservoir, which is the relevant case for CO<sub>2</sub> sequestration.) The bounding layer is everywhere impermeable

apart from a sink of width  $W$  and permeability  $k_f$  at a distance  $x_f$  from the source. We consider separately the cases of a downslope sink and an upslope sink. We assume that the depth of the porous medium is large compared to the depth of the gravity current  $h(x, t)$  and thus neglect any motion of the ambient fluid. We also assume that the interface of the current,  $y = h(x, t)$ , is sharp, thereby neglecting any interfacial energy between the injected and ambient fluids or differences in viscosity, as is typical of buoyancy-driven flow (Lake 1989). While the capillary forces between  $\text{CO}_2$  and brine can be significant, multiphase models find that the small aspect ratio, typical of buoyancy-driven flows, leads to a balance between gravity and capillary forces (Gasda, Nordbotten & Celia 2009; Golding *et al.* 2011). The behaviour of these multiphase currents is qualitatively similar to the sharp-interface approximation employed here, and therefore, capillarity is unlikely to affect our results qualitatively.

When flow is predominantly along the slope the pressure within the current is hydrostatic,

$$P(x, y) = P_0 + x\rho g \sin \theta + \Delta\rho gh(x, t) \cos \theta - (\rho + \Delta\rho)gy \cos \theta, \tag{2.1}$$

where  $P_0$  is a constant. The along-slope Darcy velocity (Bear 1988) is

$$u = -\frac{k}{\mu} \left[ \frac{\partial P}{\partial x} - (\rho + \Delta\rho)g \sin \theta \right], \tag{2.2}$$

which, when combined with a local statement of mass conservation, determines the evolution equation for the spreading current

$$\frac{\partial h}{\partial t} - \gamma \frac{\partial}{\partial x} \left( h \frac{\partial h}{\partial x} - h \tan \theta \right) = -v_f. \tag{2.3}$$

Here,  $\gamma = kg \cos \theta \Delta\rho / \mu \phi$  is the buoyancy velocity and  $v_f$  is the leakage velocity, driven by the hydrostatic pressure gradient within the fissure (see Acton, Huppert & Worster 2001; Pritchard *et al.* 2001; Neufeld *et al.* 2009), which is given by

$$v_f = \begin{cases} 0, & |x \mp x_f| > \frac{W}{2}, \\ \gamma \frac{k_f}{k} \left[ 1 + \frac{h}{b} \right], & |x \mp x_f| < \frac{W}{2}, \end{cases} \tag{2.4}$$

with the  $\mp$  is chosen according to whether the sink is downslope ( $-$ ) or upslope ( $+$ ) of the source. Equation (2.3) is subject to boundary conditions

$$\left[ \gamma h \frac{\partial h}{\partial x} \right]_{x=0^-}^{x=0^+} = -q_{in} \quad \text{and} \quad \left[ h \frac{\partial h}{\partial x} - h \tan \theta \right]_{x_N^\pm} = 0, \tag{2.5a,b}$$

which describe the input flux  $q_{in}$  at  $x=0$  and zero flux at the upslope ( $x_N^-$ ) and downslope limits ( $x_N^+$ ) of the current, respectively.

The presence of the fissure suggests a natural length scale with which to scale horizontal distances,  $X = x_f$ , as well as scales  $H$  for vertical distances and  $T$  for times, where

$$H = \sqrt{\frac{x_f q_{in}}{\gamma}} \quad \text{and} \quad T = \sqrt{\frac{x_f^3}{q_{in} \gamma}}. \tag{2.6}$$

This choice of scaling leads to three dimensionless parameters describing the fissure,

$$\lambda = \frac{k_f}{k} \frac{1}{b} \sqrt{\frac{x_f^3 \gamma}{q_{in}}}, \quad \beta = \sqrt{\frac{\gamma}{x_f q_{in}}} b \quad \text{and} \quad \epsilon = \frac{W}{x_f}, \tag{2.7a,b,c}$$

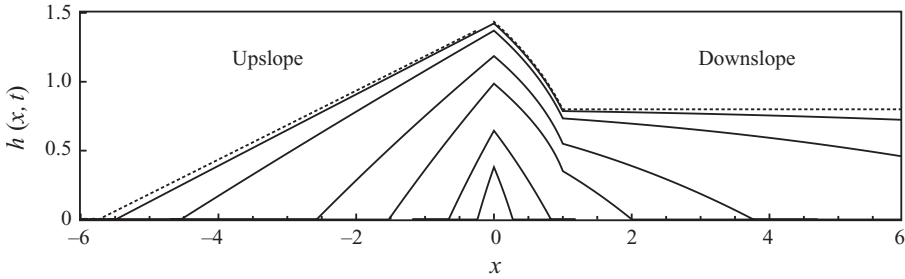


FIGURE 2. The evolution of a current flowing downslope towards a sink located at  $x_f = 1$ . Solid curves show the current shape at  $t = 0.1, 0.5, 2, 5, 20.5$  and  $52$ . The steady-state profile, determined from (3.2)–(3.5), is shown by the dashed curve. Here,  $\bar{\lambda} = 1$  and  $\sigma = 0.25$ .

which characterize the strength, vertical extent and width of the fissure, respectively. The slope of the impermeable layer is characterized by the dimensionless advection velocity

$$\sigma = \tan \theta \sqrt{\frac{\gamma x_f}{q_{in}}} = \frac{X}{H} \tan \theta. \tag{2.8}$$

In dimensionless terms, the current therefore satisfies

$$\frac{\partial h}{\partial t} - \frac{\partial}{\partial x} \left( h \frac{\partial h}{\partial x} - \sigma h \right) = \begin{cases} 0, & |x \mp 1| > \frac{\epsilon}{2}, \\ -\lambda(\beta + h), & |x \mp 1| < \frac{\epsilon}{2}, \end{cases} \tag{2.9}$$

with boundary conditions

$$\left[ h \frac{\partial h}{\partial x} \right]_{x=0^-}^{x=0^+} = -1 \quad \text{and} \quad \left[ h \frac{\partial h}{\partial x} - h \sigma \right]_{x=x_N^\pm} = 0. \tag{2.10a,b}$$

To simplify the theoretical analysis here, we set  $\beta = 0$  so that the system depends on the values of  $\sigma$ ,  $\epsilon$  and  $\lambda$  only. When comparing with experiments, however, we allow  $\beta > 0$ .

### 2.2. Efficiency of storage

A measure of considerable practical importance is the quantity of injected fluid that remains in the reservoir over time. Here, we analyze the instantaneous efficiency of storage in the reservoir,  $E_s$ , defined as the normalized difference between input and leakage fluxes. In dimensionless terms, this gives

$$E_s \equiv 1 - Q_s = 1 - \int_{\pm 1 - \epsilon/2}^{\pm 1 + \epsilon/2} \lambda h \, dx = 1 - \bar{\lambda} h_f, \tag{2.11}$$

where  $\bar{\lambda} = \epsilon \lambda$  is the width-averaged sink strength,  $h_f = \frac{1}{\epsilon} \int_{\pm 1 - \epsilon/2}^{\pm 1 + \epsilon/2} h \, dx$  is the width-averaged depth of the current over the fissure and  $Q_s = \bar{\lambda} h_f$  is the leakage flux.

### 2.3. Numerical solution

We have solved (2.9) with boundary conditions (2.10a,b) using the numerical method described by Neufeld *et al.* (2009), modified to include variable grid spacing and upwinding (Press *et al.* 1997). This variable grid spacing accounts for the asymmetric spreading of the current due to the slope. The evolution of the profile of the current is illustrated by the time series shown in figure 2. Importantly, we find that for sloping

aquifers the current tends to a steady-state profile and hence a constant efficiency of storage,  $E_s \rightarrow E_s^\infty$ . This is in contrast to the behaviour of the efficiency of storage in many horizontal geometries, which always decays to zero (Neufeld *et al.* 2009, 2011; Vella *et al.* 2011). We therefore begin by considering the steady-state profile and efficiency of storage,  $E_s^\infty$ , for both upslope and downslope sinks as a function of the advection velocity,  $\sigma$ , and the width-averaged sink strength,  $\bar{\lambda}$ .

### 3. The steady state

In the steady state, the current can be divided into three regions, each carrying its own constant volume flux: upslope of both the source and the sink (*upslope*), between the source and the sink (*interior*) and downslope of both the source and the sink (*downslope*). Since the flux  $q$  is constant within each region and the shape is steady, the profile in each of these regions is obtained by solving the first integral of (2.9)

$$h \frac{dh}{dx} - \sigma h = -q, \tag{3.1}$$

for the appropriate  $q$ . We consider separately the cases of downslope and upslope sinks.

#### 3.1. Downslope sink

When the sink is downslope of the source,  $x_f = 1$ , the upslope region is stagnant,  $q = 0$ , and the upslope profile of the current is given by

$$h(x) = h(0) + \sigma x \quad (x \leq 0). \tag{3.2}$$

The profile downslope of the sink is planar ( $dh/dx = 0$ ) with flux  $q = h_f \sigma$ , where  $h_f$  is the height of the current above the sink. However, flux conservation at the sink also implies that  $q = 1 - \bar{\lambda} h_f$ , and so the current depth above the sink is given by

$$h(1) = h_f^\infty = (\sigma + \bar{\lambda})^{-1}. \tag{3.3}$$

Therefore, we immediately have that the long-time efficiency of storage is

$$E_s^\infty = \frac{\sigma}{\sigma + \bar{\lambda}} = \left(1 + \frac{\bar{\lambda}}{\sigma}\right)^{-1} = \left(1 + \frac{W k_f}{b k} \cot \theta\right)^{-1}, \tag{3.4}$$

which is only a function of the ratio  $\bar{\lambda}/\sigma$ . This function is shown by the solid curve in figure 3. Note that  $E_s^\infty$ , expressed in terms of physical parameters, is surprisingly simple.

Finally,  $q = 1$  throughout the interior region and (3.1) must be solved with the boundary condition  $h(1) = h_f = 1/(\bar{\lambda} + \sigma)$ . The solution is

$$h(x) = \frac{1 + \Lambda_W[-A \exp\{\sigma^2(x - 1) - A\}]}{\sigma} \quad (0 < x < 1), \tag{3.5}$$

where  $\Lambda_W(x)$  is the Lambert  $W$ -function, defined as the solution of  $x = \Lambda_W e^{\Lambda_W}$ , and  $A = \bar{\lambda}/(\sigma + \bar{\lambda})$ . Figure 2 shows that this steady-state profile is recovered as the long-time limit of the numerically determined current profiles.

#### 3.2. Upslope sink

Even in the absence of leakage, a current only propagates a limited distance upslope in inclined aquifers. The profile downslope of the injection point is given by  $h = h(0) = 1/\sigma$  (Huppert & Woods 1995), which, combined with (3.2), implies that the

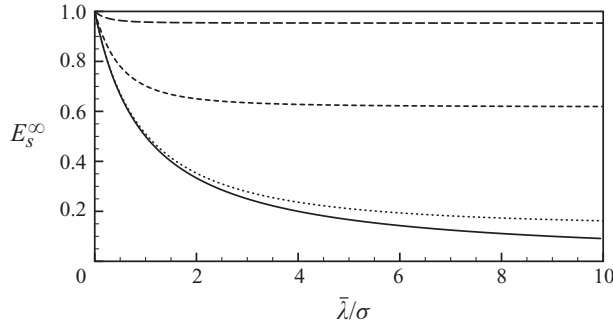


FIGURE 3. The steady-state efficiency of storage,  $E_s^\infty$ , for an upslope sink as a function of  $\bar{\lambda}/\sigma$  with  $\sigma = 0.9$  (long dash), 0.5 (short dash) and 0.1 (dotted). Note that in the limit  $\sigma \ll 1$  we recover the steady-state efficiency of storage for a downslope sink given by (3.4) (solid curve).

maximum upslope extent of the current in the absence of leakage is  $x_N^- = -1/\sigma^2$ . Thus, for  $\sigma > 1$ , the current does not reach the fissure and its development follows that detailed by Huppert & Woods (1995). For  $\sigma < 1$ , the current does reach the upslope sink and the determination of its profile follows that outlined for the downslope sink. In the stagnant region upslope of the sink, the profile is given by

$$h(x) = h_f + \sigma(1 + x) \quad (x < -1), \tag{3.6}$$

and the upslope extent is given by  $x_N^- = -(1 + h_f/\sigma)$ . The flux in the downslope region is  $q = 1 - \bar{\lambda}h_f$ , and so the depth of the downslope current is given by

$$h(x) = \frac{1 - \bar{\lambda}h_f}{\sigma} \quad (x > 0). \tag{3.7}$$

Within the interior region ( $-1 < x < 0$ ), the profile is determined by solving (3.1) with  $q = -\bar{\lambda}h_f$  and boundary conditions  $h(-1) = h_f$ ,  $h(0) = (1 - \bar{\lambda}h_f)/\sigma$ .  $h_f$  must be determined as part of the solution of this problem. We find that

$$h(x) = -\frac{\bar{\lambda}h_f}{\sigma} \left\{ 1 + \Lambda_w \left[ -\frac{1}{\bar{\lambda}h_f} \exp\left(-\frac{1 + \sigma^2 x}{\bar{\lambda}h_f}\right) \right] \right\}, \tag{3.8}$$

$$\text{where } h_f = \frac{\sigma^2 - 1}{\bar{\lambda}} \left\{ \Lambda_w \left[ \frac{(\sigma^2 - 1)(\sigma + \bar{\lambda})}{\bar{\lambda}} \exp\left(-\frac{\sigma + \bar{\lambda}}{\bar{\lambda}}\right) \right] \right\}^{-1}. \tag{3.9}$$

The steady-state efficiency of storage may therefore be calculated from (3.9) using

$$E_s^\infty = 1 - \bar{\lambda}h_f. \tag{3.10}$$

We plot the steady-state efficiency of storage,  $E_s^\infty$ , for both upslope and downslope sinks in figure 3. Note that  $E_s \rightarrow 0$  as  $\bar{\lambda} \rightarrow \infty$  for the downslope sink, while  $E_s$  remains finite in this limit for an upslope sink. Also note that for  $\sigma \ll 1$  the result for an upslope sink (3.9) approaches the much simpler downslope result (3.3).

#### 4. Evolution towards the steady state

The evolution of the current towards the steady state described in § 3 is determined by the fully time-dependent problem (2.9). Initially, as fluid begins to spread from the injection point and spatial gradients are large,  $\partial h/\partial x \gg \sigma$ , the current is diffusion dominated; the extent  $x_N \sim t^{2/3}$  and height  $h \sim t^{1/3}$  following Huppert & Woods

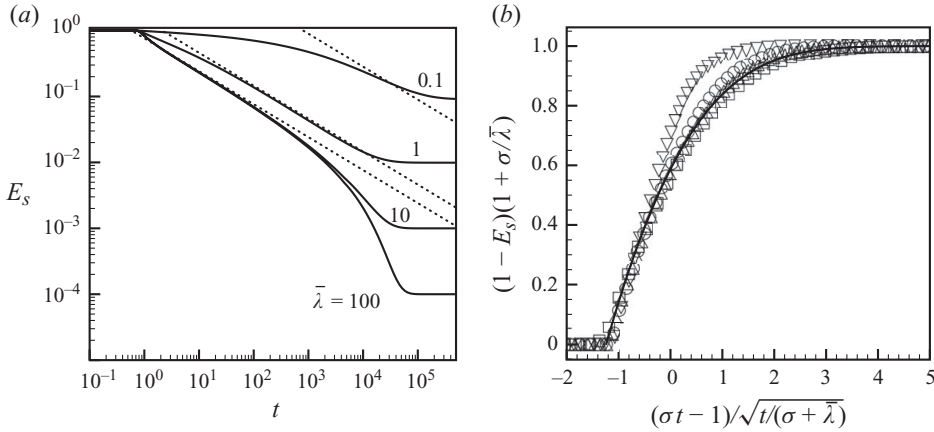


FIGURE 4. Evolution of the efficiency of storage towards the steady state value. (a) The value of  $E_s(t)$  determined by numerical simulations for  $\sigma = 10^{-2}$  with various  $\bar{\lambda}$  (curves) compared to the corresponding asymptotic results of Neufeld *et al.* (2009) for  $\sigma = 0$  (dashed lines). (b) The efficiency of storage rescaled as suggested by (4.4) for  $\sigma \gg 1$ . Here, the solid curve shows  $G(-x)$  found from the solution of (4.2) and numerical results are shown for  $\bar{\lambda} = 1$  with  $\sigma = 5$  ( $\square$ ), 1 ( $\triangle$ ), 0.5 ( $\circ$ ) and  $\sigma = 0.1$  ( $\nabla$ ).

(1995). From (2.9) we see that the advective and diffusive contributions balance when  $h/x \sim \sigma$ . This occurs at a time  $t^* \sim \sigma^{-3}$  after the start of injection by which time the current has spread a distance  $x^* \sim t^{*2/3} \sim \sigma^{-2}$  from the origin. Thus the approach to a steady-state efficiency, for a sink located at  $x_f = 1$ , is diffusively controlled when  $x^* \gg 1$  (i.e.  $\sigma \ll 1$ ) but by a balance between diffusion and along-slope advection for  $x^* \ll 1$  (i.e.  $\sigma \gg 1$ ).

#### 4.1. Diffusion dominated leakage ( $\sigma \ll 1$ )

The asymptotic efficiency of storage in the horizontal limit,  $\sigma = 0$ , was considered by Neufeld *et al.* (2009) who showed that for  $t \gg 1$

$$E_s \approx 0.444 \times [1 + (2\bar{\lambda}^2 + 1)^{3/4}] \bar{\lambda}^{-3/2} t^{-1/2}. \quad (4.1)$$

(Note that we use here the instantaneous efficiency  $E_s$  rather than the time-integrated quantity introduced by Neufeld *et al.* 2009, which modifies their prefactor by a factor of 2.) For  $\sigma \ll 1$ , we expect that the effect of the slope is minimal and hence that the efficiency of storage should follow (4.1) until the steady-state efficiency is reached,  $E_s^\infty \approx \sigma/\bar{\lambda}$ . The evolution of the efficiency of storage, along with the long-time asymptotic behaviours for the case  $\sigma = 0$ , is shown in figure 4(a). These plots confirm that the asymptotic result (4.1) gives a reasonable estimate of the evolution of  $E_s$ .

#### 4.2. Advection dominated leakage ( $\sigma \gg 1$ )

For  $\sigma \gg 1$ , the along-slope acceleration due to gravity quickly becomes important, leading to the development of the nose profile described by Huppert & Woods (1995) when the current has propagated a distance  $x^* \ll 1$ . The nose of the current therefore assumes a self-similar shape well before it encounters the fissure. To describe this profile we rewrite (2.9) in the frame of the nose by introducing  $\eta = x - \sigma t$  and  $h(x, t) = h_f^\infty [1 - g(\eta, t)]$ . The transformation of (2.9) so obtained admits a similarity

Symbol	$\nu$ (cm <sup>2</sup> s <sup>-1</sup> )	$q$ (cm <sup>2</sup> s <sup>-1</sup> )	$\theta$ (°)	$H$ (cm)	$T$ (s)	$\bar{\lambda}$	$\beta$	$\sigma$
□	7.6	3.97	9.0	4.0	10.0	0.11	1.26	0.40
○	7.6	8.25	22.3	5.9	7.2	0.07	0.85	0.70
▽	7.6	0.95	16.9	2.2	22.6	0.25	2.33	1.41
◇	7.6	1.74	16.7	2.7	15.7	0.18	1.82	1.09
×	7.6	0.95	6.4	1.9	19.8	0.26	2.37	0.53
△	4.8	6.07	18.8	4.2	6.8	0.12	1.21	0.89

TABLE 1. Summary of parameters investigated experimentally. We also have  $x_f = 10$  cm,  $b = 5$  cm and  $W = 0.7$  cm.

solution  $G(\xi) = g(\eta, t)$ , where  $\xi = \eta/(h_f^\infty t)^{1/2}$  and  $G(\xi)$  satisfies

$$-\frac{1}{2}\xi \frac{dG}{d\xi} = \frac{d}{d\xi} \left[ (1 - G) \frac{dG}{d\xi} \right]. \quad (4.2)$$

The solution of (4.2) is found subject to the boundary condition that the current depth vanishes at the nose,  $\xi = \xi_N$  in similarity variables, giving  $G(\xi_N) = 1$ . The conservation of mass gives an integral condition for  $\xi_N$ , which may be written as

$$\xi_N = \int_{-\infty}^{\xi_N} G(\xi) d\xi. \quad (4.3)$$

We note that this corrects an apparent typographical error by Huppert & Woods (1995), and find that  $\xi_N = 1.238$ . For  $\sigma \gg 1$ , the advection of this profile past the sink determines, to leading order, the efficiency of storage. We therefore find that  $E_s = 1 - \bar{\lambda}h(1, t) = 1 - \bar{\lambda}h_f^\infty [1 - g(1 - \sigma t, t)]$  and hence that

$$\frac{1 - E_s}{\bar{\lambda}h_f^\infty} = 1 - G \left[ \frac{1 - \sigma t}{(h_f^\infty t)^{1/2}} \right]. \quad (4.4)$$

Substituting the form of  $h_f^\infty$  from (3.3) provides the motivation for the plot in figure 4(b), which shows that the evolution of the efficiency of storage can indeed be understood simply by the shape of the nose sweeping over the sink.

## 5. Experimental analogue

A series of analogue laboratory experiments were conducted to test whether the efficiency of storage does indeed tend to a steady-state value. Six experiments were conducted in a Hele-Shaw cell measuring 200 cm × 30 cm × 0.5 cm. We injected glycerine using a peristaltic pump, while leakage occurred from a localized hole in the base of the tank. Digital mass balances recorded the mass of fluid injected and the total mass of fluid that had leaked as functions of time. The value of  $k_f$  was determined in a separate series of experiments with  $\sigma = 0$  in the manner described by Neufeld *et al.* (2009). The experiments reported here were all performed with a downslope sink, although comparable results were also obtained with an upslope sink. The parameters in each experimental run are summarized in table 1.

Experimental results for the evolution of  $E_s$  are shown in figure 5. These results confirm that the efficiency of storage does indeed tend to a steady-state value,  $E_s^\infty$ , as  $t \rightarrow \infty$  and that this value is well predicted by the analytical arguments presented earlier, albeit modified to allow  $\beta > 0$ . Furthermore, we see that the temporal evolution

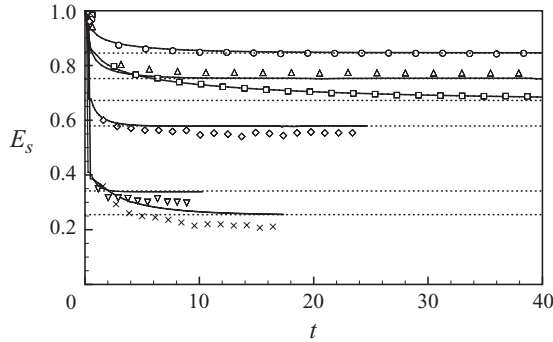


FIGURE 5. The evolution of efficiency of storage for a downslope sink as a function of dimensionless time,  $t$ . Results are shown for the experimental runs reported in table 1; the same symbols being used here. The evolution of  $E_s$  predicted by the numerical solution of (2.9) is shown by the solid curve along with the asymptotic steady-state efficiency (dashed horizontal lines).

of  $E_s$  towards  $E_s^\infty$  is reasonably well described by the numerical solution of (2.9). In performing the comparison between theory and experiment it was necessary to account for the basal drag of the Hele-Shaw cell. This was done using the modified permeability described by Neufeld *et al.* (2009) to account for this departure from Darcy flow. (Note that the injected volume flux was determined from a linear fit of the injected mass eliminating small fluctuations caused by the peristaltic pump. The leakage flux was determined by using linear fits to consecutive epochs of data, each 10 s in duration.)

## 6. Discussion

We now turn to discuss the relevance of our results for the geological storage of  $\text{CO}_2$ . In carbon capture and storage schemes,  $\text{CO}_2$  is captured, compressed and finally injected into geological reservoirs at depths typically greater than 1000 m. At these depths the pressure and temperature are such that  $\text{CO}_2$  is a supercritical fluid but remains buoyant with respect to the ambient brine. It therefore rises until it encounters a region of lower permeability (a cap rock) where it spreads as a gravity current (Huppert 2006).

It is informative to determine the time scales over which significant leakage occurs, for comparison with the time scales for secondary trapping mechanisms such as dissolution and residual trapping. We therefore determine  $t_{90}$ , the time taken for  $E_s$  to reach 90%, and its dependence on  $\bar{\lambda}$  and  $\sigma$ . A contour plot of  $t_{90}$  is shown in figure 6(a). We note that for  $\sigma > 9\bar{\lambda}$ ,  $t_{90} = \infty$  – the system remains at efficiencies greater than 90% for all times because  $E_s^\infty > 90\%$ . For  $\sigma \ll 1$ ,  $t_{90}$  depends only on  $\bar{\lambda}$ , as expected. Furthermore, we observe the  $t_{90} \sim \bar{\lambda}^{-3}$  scaling predicted by (4.1) for  $\bar{\lambda} \ll 1$  (figure 6b). For  $\bar{\lambda} \gg 1$ ,  $t_{90}$  depends only on  $\sigma$  and, in the limit  $\sigma \gg 1$ , is given approximately by the time for advection to take the current to the sink,  $t_{90} \approx \sigma^{-1}$  (figure 6c).

We note that the primary unknowns in a practical scenario are likely to be  $x_f$ ,  $W$  and  $b$ . For simplicity, we shall assume that  $W = b$  and  $k_f = k$ , so that the ratio  $\sigma/\bar{\lambda} = \tan \theta$  is independent of the distance to the fissure/fracture  $x_f$  or, indeed, any other property of the system. In a given field, we imagine that robust estimates of  $\theta$  are possible. The main uncertainty therefore lies in the distance between the source

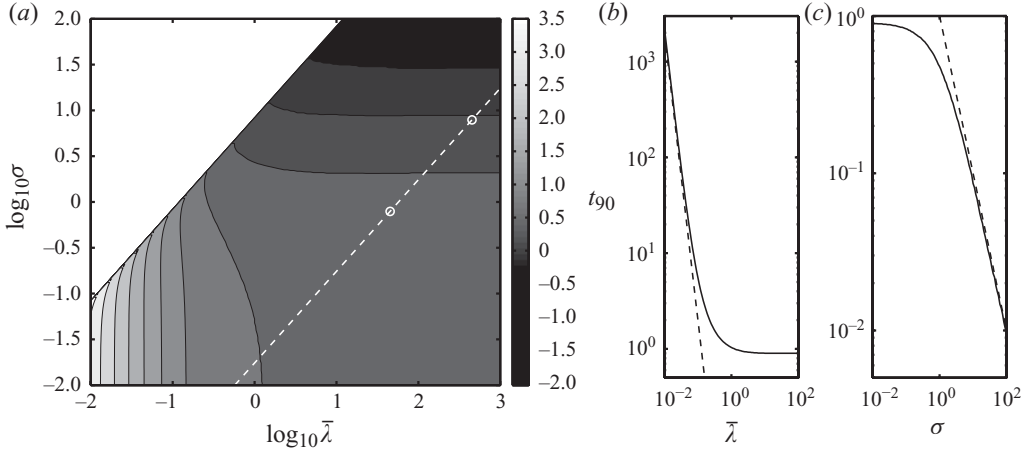


FIGURE 6. The dependence of  $t_{90}$  on the parameters  $\bar{\lambda}$  and  $\sigma$ . (a) Contour plot (on logarithmic axes) showing  $\log_{10} t_{90}$ , (b)  $t_{90}(\bar{\lambda})$  for  $\sigma \ll 1$  (solid curve) with scaling  $t_{90} \sim \bar{\lambda}^{-3}$  (dashed line) and (c)  $t_{90}(\sigma)$  for  $\bar{\lambda} \gg 1$  (solid curve) with scaling  $t_{90} \sim \sigma^{-1}$ . In (a) the dashed line shows the allowed values of  $\sigma$  and  $\bar{\lambda}$  for  $b=W, \theta=1^\circ$  while the two points show  $x_f=100$  m and  $x_f=10$  km, respectively, for Sleipner.

and the fissure. For a given  $\theta$ ,  $t_{90}$  varies along the line  $\sigma = \bar{\lambda} \tan \theta$  in the contour plot of figure 6(a). However, to get concrete values we must use specific values for a given setup. The largest sequestration project currently operational, though still a demonstration, is that at Sleipner, Norway. Here  $1 \text{ MT year}^{-1}$  of  $\text{CO}_2$  is injected into the Utsira formation, a sandstone with permeability  $k \approx 3.05 \times 10^{-12} \text{ m}^2$  and porosity  $\phi = 0.3$  (Bickle *et al.* 2007). At this depth, the densities of the injected and ambient fluids are  $\rho_{\text{CO}_2} \approx 515 \text{ kg m}^{-3}$  and  $\rho_{\text{brine}} \approx 1020 \text{ kg m}^{-3}$ . The viscosity of the injected  $\text{CO}_2$  is believed to be  $\mu \approx 4 \times 10^{-5} \text{ Pa s}$  (Bickle *et al.* 2007). We therefore have that  $\gamma \approx 1 \times 10^{-3} \text{ ms}^{-1}$ , and the effective two-dimensional flux (averaged over a width of 1 km) is  $q \approx 6 \times 10^{-5} \text{ m}^2 \text{ s}^{-1}$ . It is then a simple matter to plot points on the contour plot corresponding to  $x_f = 100$  m and 10 km for  $\theta = 1^\circ$ . Such a plot is shown in figure 6(a). We find that the dimensional values of  $t_{90}$  are 0.06 year ( $x_f = 100$  m) and 13 years ( $x_f = 10$  km). These values should be compared to the corresponding values in the absence of a slope for which we find that  $t_{90} = 0.1$  year and  $t_{90} = 102$  years, respectively. Therefore, while the presence of a sloping cap rock ensures that the efficiency of storage is bounded below by a finite value, it may also reduce the time taken to reach a given efficiency of storage. This delicate balance is likely to be important when considering sloping cap rocks in real-world carbon sequestration and hence deserves further study.

This work is supported by an Oppenheimer Early Career Fellowship (D.V.) as well as by a Lloyd's Tercentenary Fellowship and a Leverhulme Early Career Fellowship (J.A.N.). We are grateful to Mark Hallworth for his technical assistance.

#### REFERENCES

- ACTON, J., HUPPERT, H. E. & WORSTER, M. G. 2001 Two-dimensional viscous gravity currents flowing over a deep porous medium. *J. Fluid Mech.* **440**, 359–380.  
 BEAR, J. 1988 *Dynamics of Fluids in Porous Media*. Dover.

- BICKLE, M., CHADWICK, A., HUPPERT, H. E., HALLWORTH, M. A. & LYLE, S. 2007 Modelling carbon-dioxide accumulation at Sleipner: implications for underground carbon storage. *Earth Planet. Sci. Lett.* **255**, 164–176.
- GASDA, S. E., NORDBOTTEN, J. M. & CELIA, M. A. 2009 Vertical equilibrium with sub-scale analytical methods for geological CO<sub>2</sub> sequestration. *Comput. Geosci.* **13**, 469–481.
- GOLDING, M. J., NEUFELD, J. A., HESSE, M. A. & HUPPERT, H. E. 2011 Two-dimensional gravity currents in porous media. *J. Fluid Mech.* (in press).
- HUPPERT, H. E. 2006 Gravity currents: a personal perspective. *J. Fluid Mech.* **554**, 299–322.
- HUPPERT, H. E. & WOODS, A. W. 1995 Gravity-driven flows in porous layers. *J. Fluid Mech.* **292**, 55–69.
- LAKE, L. 1989 *Enhanced Oil Recovery*. Prentice Hall.
- LYLE, S., HUPPERT, H. E., HALLWORTH, M. A., BICKLE, M. & CHADWICK, A. 2005 Axisymmetric gravity currents in a porous medium. *J. Fluid Mech.* **543**, 293–302.
- NEUFELD, J. A., VELLA, D. & HUPPERT, H. E. 2009 The effect of a fissure on storage in a porous medium. *J. Fluid Mech.* **639**, 239–259.
- NEUFELD, J. A., VELLA, D., HUPPERT, H. E., & LISTER, J. R. 2011 Leakage from gravity currents in a porous medium. Part 1. A localized sink. *J. Fluid Mech.* **666**, 391–413.
- PRESS, W. H., TEUKOLSKY, S. A., VETTERLING, W. T. & FLANNERY, B. P. 1997 *Numerical Recipes in Fortran 77: The Art of Scientific Computing*, 2nd edn. Cambridge University Press.
- PRITCHARD, D., WOODS, A. W. & HOGG, A. J. 2001 On the slow draining of a gravity current moving through a layered permeable medium. *J. Fluid Mech.* **444**, 23–47.
- PRITCHARD, D. 2007 Gravity currents over fractured substrates in a porous medium. *J. Fluid Mech.* **584**, 415–431.
- VELLA, D., NEUFELD, J. A., HUPPERT, H. E. & LISTER, J. R. 2011 Leakage from gravity currents in a porous medium. Part 2. A line sink. *J. Fluid Mech.* **666**, 414–427.
- VELLA, D. & HUPPERT, H. E. 2006 Gravity currents in a porous medium at an inclined plane. *J. Fluid Mech.* **555**, 353–362.
- WOODS, A. W. & FARCAS, A. 2009 Capillary entry pressure and the leakage of gravity currents through a sloping layered permeable rock. *J. Fluid Mech.* **618**, 361–379.